nature medicine

Neutrophils promote Alzheimer's disease–like pathology and cognitive decline via LFA-1 integrin

Elena Zenaro[1,6], Enrica Pietronigro[1,6], Vittorina Della Bianca[1], Gennj Piacentino[1], Laura Marongiu[1], Simona Budui[1], Ermanna Turano[2], Barbara Rossi[1], Stefano Angiari[1], Silvia Dusi[1], Alessio Montresor[1,3], Tommaso Carlucci[1], Sara Nanì[1], Gabriele Tosadori[1,3], Lucia Calciano[4], Daniele Catalucci[5], Giorgio Berton[1], Bruno Bonetti[2] & Gabriela Constantin[1,3]

Inflammation is a pathological hallmark of Alzheimer's disease, and innate immune cells have been shown to contribute to disease pathogenesis. In two transgenic models of Alzheimer's disease (5xFAD and 3xTg-AD mice), neutrophils extravasated and were present in areas with amyloid-β (Aβ) deposits, where they released neutrophil extracellular traps (NETs) and IL-17. $A\beta_{42}$ peptide triggered the LFA-1 integrin high-affinity state and rapid neutrophil adhesion to integrin ligands. *In vivo*, LFA-1 integrin controlled neutrophil extravasation into the CNS and intraparenchymal motility. In transgenic Alzheimer's disease models, neutrophil depletion or inhibition of neutrophil trafficking via LFA-1 blockade reduced Alzheimer's disease–like neuropathology and improved memory in mice already showing cognitive dysfunction. Temporary depletion of neutrophils for 1 month at early stages of disease led to sustained improvements in memory. Transgenic Alzheimer's disease model mice lacking LFA-1 were protected from cognitive decline and had reduced gliosis. In humans with Alzheimer's disease, neutrophils adhered to and spread inside brain venules and were present in the parenchyma, along with NETs. Our results demonstrate that neutrophils contribute to Alzheimer's disease pathogenesis and cognitive impairment and suggest that the inhibition of neutrophil trafficking may be beneficial in Alzheimer's disease.

Alzheimer's disease is the most common form of dementia. It affects more than 35 million people worldwide[1]. It is characterized by a progressive deterioration of cognitive function, and the neuropathological features include Aβ plaques, neurofibrillary tangles comprising aggregates of hyperphosphorylated tau, amyloid angiopathy, neuronal loss and synaptic dysfunction[1,2]. A large body of evidence suggests that Alzheimer's disease is promoted by inflammation and innate immune mechanisms of the central nervous system (CNS)[3–7]. Chronic inflammatory disorders in humans, including atherosclerosis, obesity, diabetes and periodontitis, either represent risk factors for or are associated with late-onset Alzheimer's disease[6]. Accordingly, epidemiological studies have suggested that nonsteroidal anti-inflammatory drugs (NSAIDs) reduce the risk of Alzheimer's disease, thus confirming its link with inflammation[8,9]. Even so, several prospective placebo-controlled trials to test the efficacy of NSAIDs against Alzheimer's disease have failed, suggesting that specific inflammatory pathways need to be identified and targeted[3,5,9].

It is widely accepted that microglia-mediated neuroinflammatory responses may promote neurodegeneration in Alzheimer's disease[3,10]. Microglial activation precedes neuropil loss in patients with Alzheimer's disease, and recent genome-wide association studies have revealed that microglial genes such as *CD33*, *TREM2* and *HLA-DR* are associated with susceptibility to late-onset Alzheimer's disease[11–15]. Activated microglia can induce highly detrimental neurotoxic effects, and hence the attenuation of the microglial response has been proposed as a potential therapeutic approach in Alzheimer's disease[10].

Vascular inflammation and a dysfunctional blood-brain-barrier (BBB) have been implicated in the pathogenesis of Alzheimer's disease[16,17]. Blood-derived leukocyte subpopulations, including lymphocytes, monocytes and neutrophils, have been identified in the brains of patients with Alzheimer's disease and in corresponding animal models[3,4,18–22]. Whereas blood monocytes have been associated with Aβ clearance[22], the role of other circulating leukocytes in the induction of neuropathological changes and memory deficit associated with Alzheimer's disease remains unclear.

RESULTS

Vascular adhesion molecules are expressed in disease models

We performed confocal microscopy experiments on brain sections of 5xFAD mice, which overexpress mutant human APP(695) with the Swedish (K670N, M671L), Florida (I716V) and London (V717I) familial Alzheimer's disease (FAD) mutations and human PS1 harboring the two FAD mutations M146L and L286V. These mice accumulate Aβ deposits by 2 months of age and exhibit memory impairment starting at 4 months of age[23]. We found that the expression of E-selectin,

[1]Department of Pathology and Diagnostics, University of Verona, Verona, Italy. [2]Department of Neurological and Movement Sciences, Neurology Section, University of Verona, Verona, Italy. [3]The Center for Biomedical Computing (CBMC), University of Verona, Verona, Italy. [4]Department of Public Health and Community Medicine, University of Verona, Verona, Italy. [5]National Research Council (CNR), Institute of Genetic and Biomedical Research (IRGB), and Humanitas Research Hospital, Milan, Italy. [6]These authors contributed equally to this work. Correspondence should be addressed to G.C. (gabriela.constantin@univr.it).

Received 23 December 2014; accepted 29 June 2015; published online 27 July 2015; doi:10.1038/nm.3913

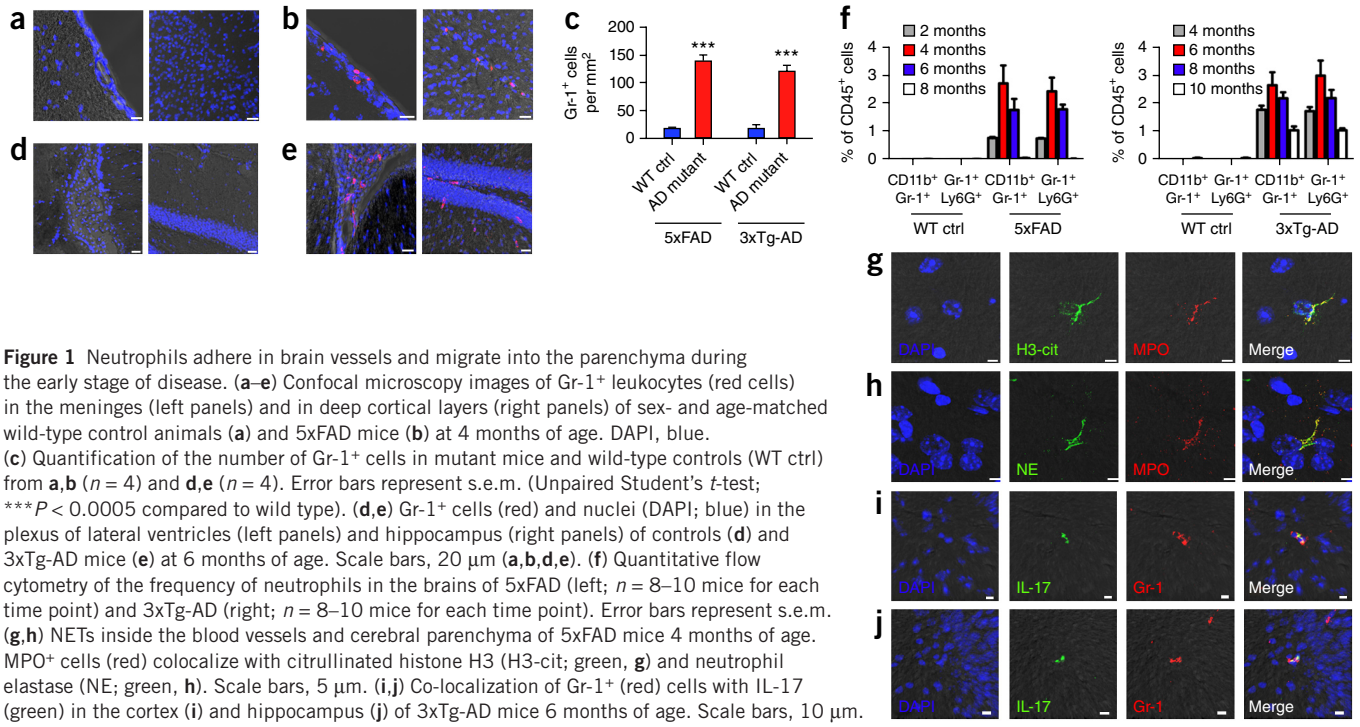

Figure 1 Neutrophils adhere in brain vessels and migrate into the parenchyma during the early stage of disease. (**a**–**e**) Confocal microscopy images of Gr-1$^+$ leukocytes (red cells) in the meninges (left panels) and in deep cortical layers (right panels) of sex- and age-matched wild-type control animals (**a**) and 5xFAD mice (**b**) at 4 months of age. DAPI, blue. (**c**) Quantification of the number of Gr-1$^+$ cells in mutant mice and wild-type controls (WT ctrl) from **a**,**b** ($n = 4$) and **d**,**e** ($n = 4$). Error bars represent s.e.m. (Unpaired Student's *t*-test; $^{***}P < 0.0005$ compared to wild type). (**d**,**e**) Gr-1$^+$ cells (red) and nuclei (DAPI; blue) in the plexus of lateral ventricles (left panels) and hippocampus (right panels) of controls (**d**) and 3xTg-AD mice (**e**) at 6 months of age. Scale bars, 20 µm (**a**,**b**,**d**,**e**). (**f**) Quantitative flow cytometry of the frequency of neutrophils in the brains of 5xFAD (left; $n = 8$–10 mice for each time point) and 3xTg-AD (right; $n = 8$–10 mice for each time point). Error bars represent s.e.m. (**g**,**h**) NETs inside the blood vessels and cerebral parenchyma of 5xFAD mice 4 months of age. MPO$^+$ cells (red) colocalize with citrullinated histone H3 (H3-cit; green, **g**) and neutrophil elastase (NE; green, **h**). Scale bars, 5 µm. (**i**,**j**) Co-localization of Gr-1$^+$ (red) cells with IL-17 (green) in the cortex (**i**) and hippocampus (**j**) of 3xTg-AD mice 6 months of age. Scale bars, 10 µm.

P-selectin, vascular cell adhesion molecule-1 (VCAM-1) and intercellular adhesion molecule-1 (ICAM-1) was higher in 4-month-old mice than in sex- and age-matched wild-type controls. These adhesion molecules were expressed mainly in the vessels of the meninges and cortex, but also in the choroid plexus, hippocampus and amygdala of the mutant mice (**Supplementary Fig. 1a**,**b**,**e** and data not shown). We excluded the possibility that adhesion molecule expression was dependent on the experimental model by repeating the analysis in 3xTg-AD mice expressing transgenes for three mutant human proteins: PS1 (M146V), βAPP (Swedish) and tau (P301L). We observed high expression of all vascular adhesion molecules compared to that in sex- and age-matched controls in the hippocampus and cortex at 6 months of age (**Supplementary Fig. 1c**,**d**,**f** and data not shown). At this age 3xTg-AD mice show amyloid deposits in the neocortex, hippocampus and amygdala, accumulate phosphorylated tau in the hippocampus, and develop synaptic dysfunction and memory loss[24–29]. Adhesion molecules were also expressed at 2 and 8 months of age in 5xFAD mice and at 4 and 10 months of age in 3xTg-AD mice, suggesting that vascular inflammation may play a continual pathogenic role (data not shown). Adhesion molecule expression was often found in close proximity to Aβ deposits (**Supplementary Fig. 1g**–**j**), and additional *in vitro* experiments confirmed that $A\beta_{42}$ peptide induced the expression of adhesion molecules in brain endothelial cell lines without affecting cell viability (**Supplementary Fig. 1k**–**m**).

Neutrophils migrate into brain and produce NETs and IL-17

More CD45$^+$ and CD18$^+$ cells were observed in animals with cognitive impairment than in sex- and age-matched wild-type littermates, and they were primarily localized around meningeal and cortical vessels or adhering inside blood vessels in 4-month-old 5xFAD mice or in the choroid plexuses, cortex and hippocampus in 6-month-old 3xTg-AD mice (**Supplementary Fig. 2a**–**h** and data not shown). Cells expressing granulocyte receptor 1 (Gr-1) adhering to blood vessels or migrating inside the parenchyma were present in the same areas as CD45$^+$ or CD18$^+$ cells, suggesting that most of the migrating cells were neutrophils (**Fig. 1a**–**f** and data not shown).

The presence of neutrophils in the brains of Alzheimer's disease model mice was confirmed using an anti-Ly6G antibody. The number of Ly6G$^+$ cells was increased in the brains of mutant mice compared to wild-type controls (**Supplementary Fig. 2j**–**o**). Neutrophils stained for naphthol AS-D chloroacetate esterase, which is specific for cells of the granulocytic lineage, accumulated in the brains of 3xTg-AD mice, whereas no stained cells were found in wild-type animals (**Supplementary Fig. 2p**), further confirming the accumulation of this leukocyte subtype in Alzheimer's models.

Next we analyzed the kinetics of Gr-1$^+$ leukocyte accumulation in the brains of model mice (**Fig. 1f** and **Supplementary Fig. 3a**). Most Gr-1$^+$ cells were also positive for Ly6G in the CD45$^+$ or CD18$^+$ cell populations, confirming that the Gr-1$^+$ cells migrating into the brains of mice with Alzheimer's disease–like pathology are neutrophils (**Fig. 1f** and **Supplementary Fig. 3b**,**c**). Neutrophil infiltration peaked at 4 and 6 months of age in 5xFAD and 3xTg-AD mice, respectively, coinciding with the onset of memory loss in cognitive tests (**Fig. 1f** and data not shown)[23,24]. Neutrophils also accumulated before the onset of cognitive deficits and at 8–10 months of age, especially in older 3xTg-AD mice, compared to healthy controls (**Fig. 1f**), suggesting that neutrophils play a role in the induction of cognitive decline as well as in disease progression.

The release of NETs induces microbial killing during infection and tissue destruction during sterile inflammation[30,31]. Cells releasing myeloperoxidase (MPO), neutrophil elastase and citrullinated histone H3 were present in the parenchyma (**Fig. 1g**,**h**) and blood vessels (data not shown) of mouse models of Alzheimer's disease. Migrating neutrophils in the cortex and hippocampus produced IL-17 (**Fig. 1i**,**j**), a cytotoxic cytokine for neurons that may alter the BBB[32,33].

In vivo imaging of neutrophil trafficking in model mice

Next we conducted two-photon laser-scanning microscopy (TPLSM) experiments in the cortex of 5xFAD mice (**Fig. 2a**,**b**). Exogenous labeled

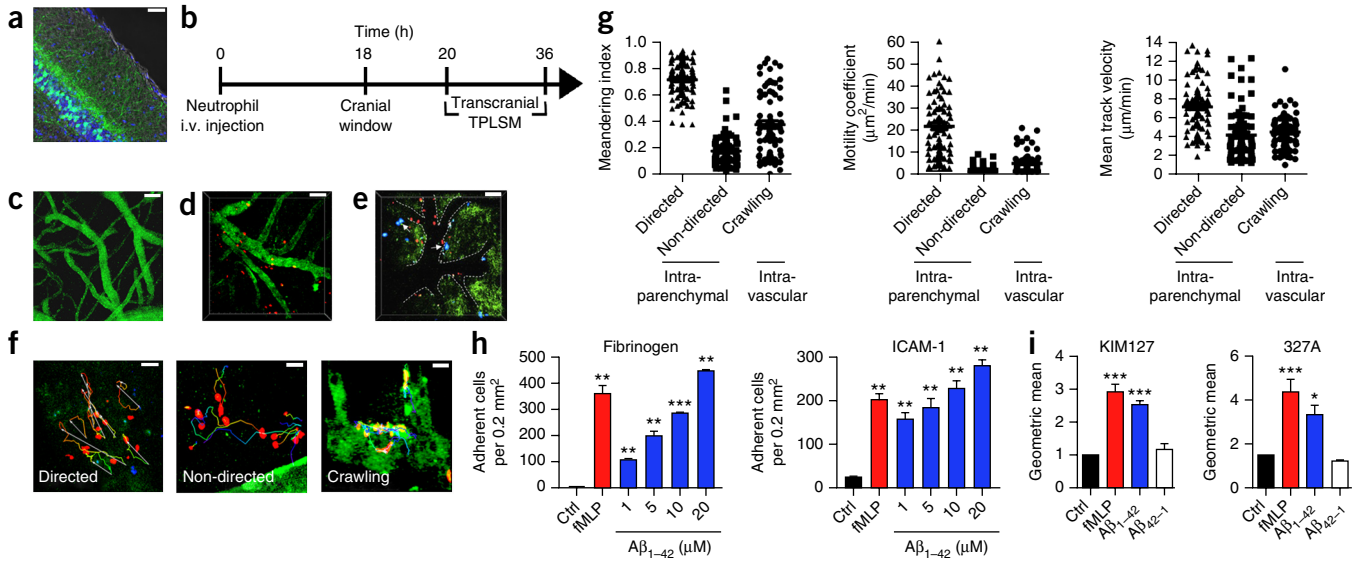

Figure 2 Neutrophils traffic into the brain and Aβ triggers neutrophil adhesion. (**a**) Somatosensory cortical portion used for TPLSM experiments in the cortex of a 5xFAD-YFPH mouse, with YFPH neurons (green) and cell nuclei (blue). Scale bar, 30 μm. (**b**) Timeline of TPLSM experiments; i.v., intravenous. (**c**,**d**) Representative TPLSM images in wild-type (**c**) and 5xFAD mice (**d**) of migrating neutrophils (red) in the parenchyma or of adherent and crawling cells (red) inside the blood vessels (green). (**e**) Confocal image of neutrophils (red), Aβ (blue) and neurons (green) in the 5xFAD-YFPH mouse cortex. Arrows, Aβ plaques; dashed lines, vessel edges. (**f**) Representative TPLSM images showing intraparenchymal directed and non-directed cells and intravascular crawling cells with movement tracking. The movement of a given cell is represented by a colored path, with the time dimension encoded by its color (blue to red). Vectors in the left panel indicate the directed movement. Red, neutrophils; green, blood vessels. Scale bars, 50 μm (**c**–**e**) and 20 μm (**f**). (**g**) Movement parameters of intravascular and intraparenchymal neutrophils. (**h**) Soluble oligomeric Aβ triggers rapid human neutrophil adhesion to fibrinogen and ICAM-1. Values are expressed as the mean counts of adhered cells in 0.2 mm^2 from three experiments. Error bars represent s.e.m. (**$P < 0.001$; ***$P < 0.0001$; Mann-Whitney test). (**i**) LFA-1 affinity state, detected with the KIM127 antibody for the low- to intermediate-affinity state and the 327A antibody for the high-affinity state. Values represent geometric mean of fluorescence intensities measured by flow cytometry, normalized against the untreated control (Ctrl) condition for each experiment. Bars represent means ± s.e.m. for three independent experiments. (ANOVA followed by Bonferroni's *post hoc* test) (*$P < 0.01$; **$P < 0.001$; ***$P < 0.0001$).

neutrophils adhered to the vascular endothelium and migrated into the brain parenchyma, whereas neutrophils were unable to adhere or extravasate in age-matched wild-type animals (**Fig. 2c**,**d** and **Supplementary Video 1**). Neutrophils crawled on the endothelium (**Fig. 2f**,**g** and **Supplementary Video 2**), potentially seeking optimal sites for emigration. Furthermore, neutrophils migrating into the parenchyma showed two different behaviors. The first involved a strong directional bias characterized by a high meandering index (Online Methods; 0.73 ± 0.24, mean ± s.d.), motility coefficient (Online Methods; 20.84 ± 14.79 μm^2/min, mean ± s.d.) and mean track velocity (6.89 ± 2.78 μm/min, mean ± s.d.) (**Fig. 2f**,**g** and **Supplementary Video 3**). The second was characterized by low motility and undirected movement resembling swarming behavior (**Fig. 2f**,**g** and **Supplementary Video 4**). Notably, more than 40% of the undirected intraparenchymal

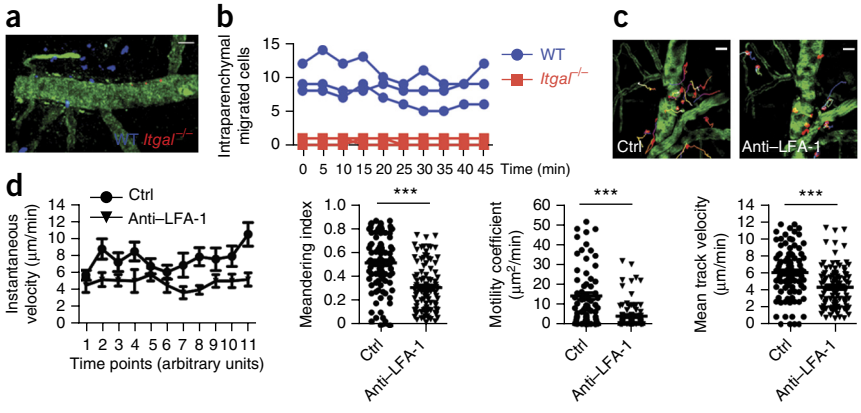

Figure 3 LFA-1 integrin is necessary for neutrophil trafficking into the brain in Alzheimer's disease models. (**a**) Representative images from TPLSM experiments with wild-type (WT) neutrophils (blue cells, labeled with CMAC (7-amino-4-chloromethylcoumarin)) migrating into the brain parenchyma of 5xFAD mice. *Itgal*$^{-/-}$ neutrophils (red cells, labeled with CMTPX) are confined to the blood vessel (green). Scale bar, 50 μm. (**b**) Quantification of intraparenchymal wild-type and *Itgal*$^{-/-}$ neutrophils. Each line shows the number of intraparenchymal migrating cells from a single mouse. The data are from one representative experiment with three mice per condition from a series of three experiments with similar results. (**c**) Cortical blood vessels were labeled in green using 525-nm non-targeted quantum dots before image acquisition. After 1–2 h during which neutrophil movement was monitored (untreated control, Ctrl), LFA-1 was blocked by administering a single intravenous dose of 200 μg anti–LFA-1 monoclonal antibody (clone TIB213). After 20 min, image acquisition was restarted in the same areas to determine how blocking LFA-1 affected neutrophil motility. Data represented as in **Figure 2f**. Images reflect one representative experiment from a series of three with similar results. Scale bars, 30 μm. (**d**) Analysis of cell motility parameters obtained with Imaris software after the injection of an anti–LFA-1 or isotype control antibody. The data show 100 manually tracked cells from one representative experiment with three mice from a series of three experiments with similar results (***$P < 0.0005$; Mann-Whitney test). Error bars, s.e.m.

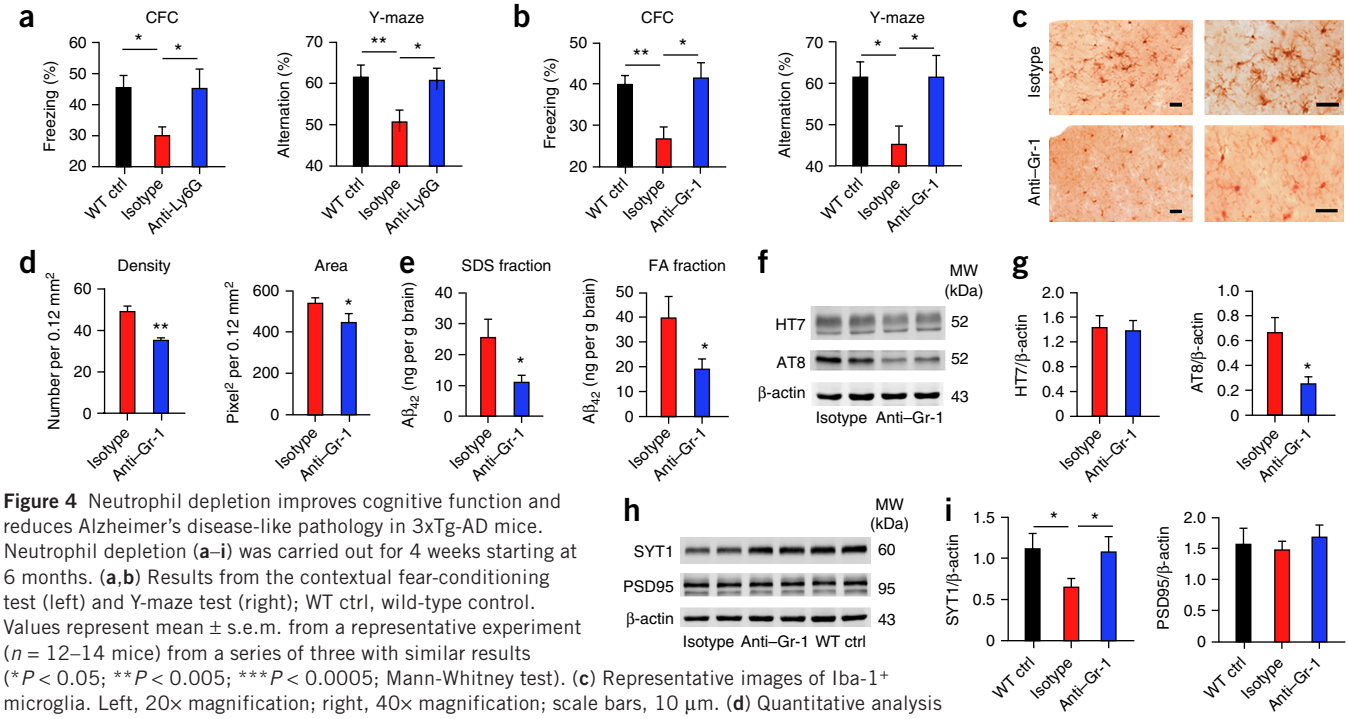

Figure 4 Neutrophil depletion improves cognitive function and reduces Alzheimer's disease-like pathology in 3xTg-AD mice. Neutrophil depletion (**a**–**i**) was carried out for 4 weeks starting at 6 months. (**a**,**b**) Results from the contextual fear-conditioning test (left) and Y-maze test (right); WT ctrl, wild-type control. Values represent mean ± s.e.m. from a representative experiment (n = 12–14 mice) from a series of three with similar results (*P < 0.05; **P < 0.005; ***P < 0.0005; Mann-Whitney test). (**c**) Representative images of Iba-1$^+$ microglia. Left, 20× magnification; right, 40× magnification; scale bars, 10 µm. (**d**) Quantitative analysis of Iba-1$^+$ cells (n = 6). Error bars indicate s.e.m. (*P < 0.05 and **P < 0.005; Mann-Whitney test). (**e**) $A\beta_{1-42}$ measured in the brains of mice treated with anti–Gr-1 (n = 8) and control (n = 6) antibodies following extraction in 2% sodium dodecyl sulfate (SDS) or in 70% formic acid (FA). Each bar represents mean ± s.e.m. (*P < 0.05; Mann-Whitney test). (**f**,**g**) Immunoblot of tau phosphorylation epitopes (AT8 antibody, detecting phospho-Ser202 and/or phospho-Thr205 tau) and total tau (HT7 antibody) (n = 7 brains per group) (**f**) and densitometric analysis (**g**). Individual samples were normalized to β-actin. Each bar represents mean ± s.e.m. (*P < 0.05, Mann-Whitney test). (**h**) Immunoblot analysis of synaptotagmin 1 (SYT1) and postsynaptic density protein PSD95 in brain homogenates. (**i**) Immunoblot quantification of SYT1 and PSD95 (n = 6 brains per group). Individual samples were normalized to β-actin. Each bar represents mean ± s.e.m. (*P < 0.05; Mann-Whitney test).

cells displayed full arrest, suggesting the presence of activating stop signals for neutrophils in Alzheimer's disease model mice. We observed neutrophil migration inside the parenchyma in areas with Aβ plaques and less neuronal fluorescence in 5xFAD-YFPH (yellow fluorescent protein H-line) mice injected with MeO-X04 (methoxy-X04) (**Fig. 2e** and **Supplementary Video 5**). Furthermore, the neutrophils displayed arrest and intraluminal crawling preferentially inside blood vessels with labeled Aβ deposits, and some cells underwent diapedesis adjacent to vascular Aβ deposits (**Supplementary Video 6**). The quantification of fluorescent neutrophil accumulation in brain homogenates by flow cytometry (**Supplementary Fig. 3d**) suggested that the half-life of neutrophils in the brain parenchyma is approximately 12 h.

$A\beta_{1-42}$ induces rapid LFA-1 integrin–dependent adhesion

We found that soluble oligomeric $A\beta_{1-42}$ triggered the rapid, integrin-dependent adhesion of both human (**Fig. 2h**) and mouse (**Supplementary Fig. 4a**,**b**) neutrophils on fibrinogen and ICAM-1 in a dose-dependent manner, whereas the reverse $A\beta_{42-1}$ peptide had no effect (data not shown). We used formyl-methionyl-leucyl-phenylalanine (fMLP) as a positive control for chemoattractant-induced adhesion. Fibrillar Aβ also induced rapid neutrophil adhesion, although with less efficacy than the soluble form (**Supplementary Fig. 4b**). Soluble Aβ also promoted the generation of reactive oxygen species in both human and mouse neutrophils (**Supplementary Fig. 4c**–**f**), further supporting a role for Aβ in neutrophil activation.

Both the formyl-peptide receptor antagonist boc-MLF and pertussis toxin (PTx) prevented rapid adhesion of human neutrophils induced by either fMLP or oligomeric $A\beta_{42}$, confirming that both triggers are mediated by $G\alpha_i$-coupled receptors (**Supplementary Fig. 4g**). Oligomeric $A\beta_{42}$ did not trigger the adhesion of lymphocytes, which are known to lack fMLP receptors (data not shown). We hypothesized that Aβ may trigger the intermediate-affinity and/or high-affinity states of integrin LFA-1 and therefore studied the effect of $A\beta_{1-42}$ oligomers on human LFA-1 integrin using the KIM127 and 327A conformer-specific antibodies, which recognize the intermediate-affinity and high-affinity states, respectively. $A\beta_{1-42}$, but not $A\beta_{42-1}$, triggered both the intermediate-affinity and high-affinity states of LFA-1 (**Fig. 2i**). Aβ therefore enhances interactions between LFA-1 and its endothelial ligands.

LFA-1 controls neutrophil trafficking into the brain

Neutrophils from LFA-1 deficient (*Itgal*$^{-/-}$) mice were unable to adhere or crawl in the blood vessels and thus to transmigrate into the brain parenchyma of 5xFAD mice (**Fig. 3a**,**b** and **Supplementary Video 7**). Blockade of LFA-1 integrin with a monoclonal antibody slowed the movement of extravasated cells (**Fig. 3c**,**d** and **Supplementary Video 8**), suggesting that LFA-1 integrin controls both the intravascular adhesion and intraparenchymal motility of neutrophils.

Neutrophil depletion improves memory and reduces pathology

We confirmed the role of neutrophils in Alzheimer's-like disease by depleting neutrophils using an anti-Ly6G antibody (clone 1A8) injected into the peripheral circulation in 6-month-old 3xTg-AD mice, which already show cognitive deficits (ref. 24 and data not shown). Mice treated with anti-Ly6G showed a 98% reduction in the number of blood neutrophils, with no reduction in monocytes (**Supplementary Fig. 4h**–**k**). After 4 weeks of treatment, the mice were allowed to rest for another 4 weeks and were then tested at 8 months of age. In the Y-maze spontaneous

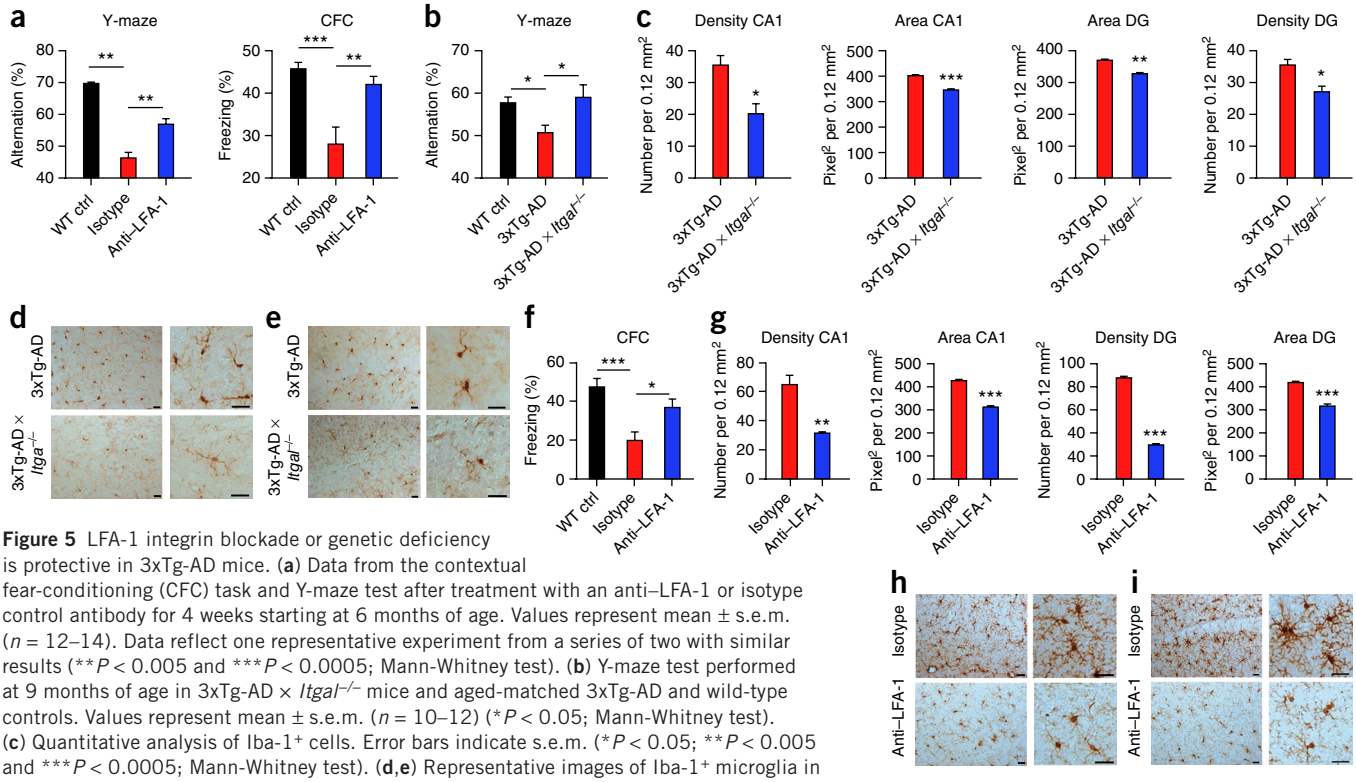

Figure 5 LFA-1 integrin blockade or genetic deficiency is protective in 3xTg-AD mice. (**a**) Data from the contextual fear-conditioning (CFC) task and Y-maze test after treatment with an anti–LFA-1 or isotype control antibody for 4 weeks starting at 6 months of age. Values represent mean ± s.e.m. (n = 12–14). Data reflect one representative experiment from a series of two with similar results (**$P < 0.005$ and ***$P < 0.0005$; Mann-Whitney test). (**b**) Y-maze test performed at 9 months of age in 3xTg-AD × *Itgal*$^{-/-}$ mice and aged-matched 3xTg-AD and wild-type controls. Values represent mean ± s.e.m. (n = 10–12) (*$P < 0.05$; Mann-Whitney test). (**c**) Quantitative analysis of Iba-1$^+$ cells. Error bars indicate s.e.m. (*$P < 0.05$; **$P < 0.005$ and ***$P < 0.0005$; Mann-Whitney test). (**d**,**e**) Representative images of Iba-1$^+$ microglia in CA1 (**d**) and dentate gyrus (DG) (**e**). (**f**) CFC in mice treated with an anti–LFA-1 or isotype control antibody for 4 weeks starting at 6 months of age and then tested after 6 months. Values represent mean ± s.e.m. (n = 10–12) (*$P < 0.05$ and ***$P < 0.0005$; Mann-Whitney test). (**g**) Quantitative analysis of Iba-1$^+$ cells at 6 months after 1 treatment with an anti–LFA-1 or isotype control antibody. Error bars indicate s.e.m. (n = 4) (**$P < 0.005$ and ***$P < 0.0005$; Student's t-test). (**h**,**i**) Representative images showing Iba-1$^+$ microglia in CA1 (**h**) and DG (**i**) of 3xTg-AD mice. Scale bars, 10 μm in **d**,**e**,**h**,**i**, left panels. Higher magnifications are shown in the right panels; scale bars, 25 μm.

alternation task and contextual fear-conditioning test, neutrophil depletion in 3xTg-AD mice with the anti-Ly6G antibody improved cognitive function to levels comparable to those in age-matched wild-type littermates (**Fig. 4a** and **Supplementary Fig. 5c**). Neutrophil depletion using an anti–Gr-1 antibody (RB6-8C5 clone) showed similar results, with significantly improved memory function in neutrophil-depleted mice compared with controls in both the above-mentioned tests (**Fig. 4b** and **Supplementary Fig. 5d**,**e**). Neutrophil depletion in 5xFAD mice using the anti–Ly 6G or anti–Gr-1 antibody for 4 weeks starting at 4 months of age, when behavioral impairments are first observed (ref. 23 and data not shown), improved performance in the Y-maze spontaneous alternation task and contextual fear-conditioning test (**Supplementary Fig. 5a**,**b**,**g**,**h**), but had no effect on the behavior of wild-type mice (data not shown).

Microgliosis, as assessed by Iba-1 staining, was less prevalent in neutrophil-depleted animals than in mice treated with the isotype control antibody (**Fig. 4c**,**d**). We observed no effect on microglia in sex- and age-matched wild-type mice after neutrophil depletion or treatment with an isotype control antibody (**Supplementary Fig. 5f**). Neutrophil depletion reduced the Aβ load in brain sections and the amount of $A\beta_{42}$ in the sodium dodecyl sulfate and formic acid fractions of brain homogenates from 3xTg-AD mice as compared to mice treated with the isotype control antibody (**Fig. 4e** and **Supplementary Fig. 5i**,**j**,**m**).

Neutrophil depletion lowered the amount of tau phosphorylated on Ser202 or Thr205 in 3xTg-AD mice (**Fig. 4f**,**g**), without changing in the total amount of tau (**Fig. 4f**,**g**). We found that the presynaptic vesicle protein synaptotagmin was depleted in mice treated with the control antibody but reached near wild-type levels in neutrophil-depleted animals (**Fig. 4h**,**i**). However, the postsynaptic plasma membrane protein PSD95 was unaffected (**Fig. 4h**,**i**).

LFA-1 inhibition reduces pathology and cognitive deficits

To interfere with neutrophil migration into the brain, we treated 6-month-old 3xTg-AD mice with an anti–LFA-1 antibody. This improved memory function, restoring performance to levels comparable to those of wild-type age-matched littermates, whereas no improvement occurred in 3xTg-AD mice treated with a control antibody (**Fig. 5a**). In 3xTg-AD mice lacking LFA-1 (3xTg-AD × *Itgal*$^{-/-}$ mice), LFA-1 deficiency prevented cognitive dysfunction in the Y-maze spontaneous alternation task, with performance comparable to that of wild-type sex- and age-matched littermates (**Fig. 5b**). Microgliosis was also reduced in the CA1 region and dentate gyrus of the hippocampus in 3xTg-AD × *Itgal*$^{-/-}$ mice compared to 3xTg-AD controls (**Fig. 5c**–**e**).

Transient, early neutrophil blockade has long-term benefits

Six-month-old 3xTg-AD mice treated with the neutrophil-depleting anti–Gr-1 antibody for 4 weeks and then tested at 6 months exhibited improved cognitive function, with performance comparable to that of healthy wild-type animals (**Supplementary Fig. 5n**). Temporarily blockade of LFA-1 during the early stages of disease also improved cognitive performance in these mice at later time points; their performance was comparable to that of wild-type littermates (**Fig. 5f**). In mice treated with antibodies against Gr-1 and LFA-1, microgliosis was reduced compared to that in mice treated with the isotype control antibody (**Fig. 5g**–**i**, **Supplementary Fig. 5o**–**q** and data not shown), as was the Aβ load (**Supplementary Fig. 5k**,**l**).

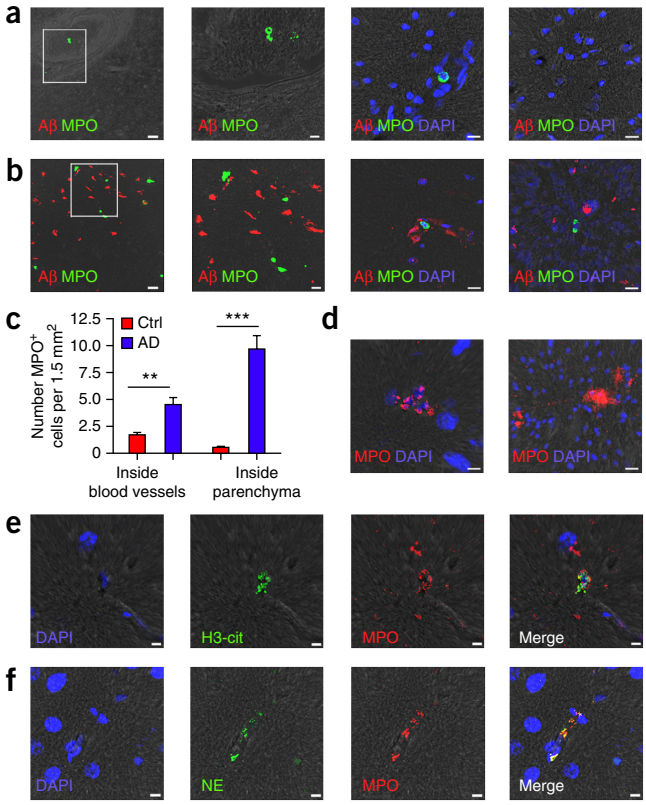

Figure 6 Neutrophils adhere in brain vessels, are present in the parenchyma and produce NETs in the brains of individuals with Alzheimer's disease. (**a**,**b**) Immunofluorescence staining of human cortex and hippocampus from age-matched control subjects (**a**) or individuals with Alzheimer's disease (**b**) with antibodies against Aβ (red) and MPO (green), with or without DAPI (blue). The outlined area in **a**,**b** (left panels) is shown at higher magnification in the adjacent panel. The right pairs of panels show MPO$^+$ cells adjacent to Aβ deposits. (**c**) Quantification of MPO$^+$ cells in brains from healthy controls ($n = 11$) and Alzheimer's disease (AD) patients ($n = 11$). Values represent the mean number of cells per 1.5 mm^2 of tissue ± s.e.m. (**$P < 0.005$; ***$P < 0.0005$; Mann-Whitney test). (**d**) MPO staining of NET-like structures found in blood vessels (left) and in the cerebral parenchyma (right). (**e**,**f**) Cell nuclei were labeled with DAPI (blue). MPO staining with avidin–Texas Red (MPO, red) colocalized with the green citrullinated histone H3 FITC (H3cit, green; **e**). Neutrophil elastase staining (NE, green) colocalized with MPO (red; **f**). Scale bars: 50 μm (**a** and **b**, left panel), 10 μm (**a** and **b**, right three panels), 5 μm (**d**, left), 15 μm (**d**, right) and 5 μm (**e** and **f**).

Neutrophils and NETs in the CNS of individuals with Alzheimer's disease

The number of MPO$^+$ cells both inside blood vessels and in the cortex and hippocampus of individuals with Alzheimer's disease were higher than in age-matched controls (**Fig. 6a–c** and **Supplementary Fig. 6a**,**b**). In individuals with Alzheimer's disease, most neutrophils had apparently migrated inside the brain parenchyma in close proximity to Aβ deposits, whereas the fewer neutrophils found in age-matched control subjects were mostly confined to the blood vessels (**Fig. 6a–c** and **Supplementary Table 1**). Neutrophils adhered to and spread inside the cortical brain vessels of individuals with Alzheimer's disease, displaying a distinct front or leading edge characteristic of cell polarization before migration (**Supplementary Fig. 6b**). The proximity of MPO$^+$ cells to amyloid deposits was not statistically random: 59% of the analyzed cells were separated from an adjacent plaque by less than 50 μm ($P < 0.00001$; $n = 105$ cells from 11 subjects; **Supplementary Fig. 6i–m**). MPO$^+$ cells releasing NETs were present in the vasculature and parenchyma of individuals with Alzheimer's disease (**Fig. 6d**). The formation of NETs was confirmed by the colocalization of MPO and citrullinated histones (**Fig. 6e**), and of MPO and neutrophil elastase (**Fig. 6f**). The presence of neutrophils was confirmed by identifying cells with polysegmented nuclei migrating perivascularly or inside the brain parenchyma (**Supplementary Fig. 6c**,**d**). The accumulation of neutrophils was further supported by specific staining for naphthol AS-D chloroacetate esterase and an anti-CD66b antibody (**Supplementary Fig. 6e–h**). A graphical abstract summarizing our findings is provided in **Supplementary Figure 6n**.

DISCUSSION

Neutrophils are the first line of defense against invading pathogens, but they are also responsible for tissue destruction during sterile inflammation[30,31,33]. Our data show expression of vascular adhesion molecules and the accumulation of neutrophils in the CNS during all stages of Alzheimer's-like disease, suggesting that neutrophil trafficking may cause chronic BBB damage and inflammation. LFA-1 integrin controls neutrophil firm arrest on the inflamed endothelium in mice with Alzheimer's disease–like pathology. Endothelial ICAM-1 engagement by neutrophil LFA-1 may induce changes in the cytoskeleton of brain endothelial cells to increase vascular permeability, an event already observed in brains affected by Alzheimer's disease[16,34–39]. We found that Aβ induced LFA1-dependent adhesion of neutrophils by triggering the transition of LFA-1 from its low-affinity state to its higher-affinity states, thus enhancing neutrophil adhesion. LFA-1 not only controls intravascular adhesion but also intraparenchymal migration; thus, formyl-peptide receptors and LFA-1, together with Aβ deposits, may promote neutrophil infiltration into the brain leading to widespread tissue damage. High-affinity LFA-1 may also provide stop signals to arrested neutrophils within the parenchyma, suggesting that high-affinity LFA-1 may be critical for neutrophil accumulation and neutrophil-dependent CNS damage during Alzheimer's disease.

Neutrophil depletion or blockade of LFA-1 integrin at the onset of clinical disease had a remarkable ability to reduce neuropathological hallmarks of disease and memory deficits in Alzheimer's-like mouse models, demonstrating a role for neutrophils in the induction of cognitive dysfunction in these models. More importantly, we also found that the temporary inhibition of neutrophils during early stages of the disease had a beneficial long-term effect in older animals, demonstrating that neutrophils are key players in the development of chronic disease.

Our data show that neutrophil depletion or the inhibition of neutrophil trafficking by blocking LFA-1 integrin dramatically reduces microglial activation. The connectivity between these two phagocytes may create several feedback loops that amplify and sustain their activation[40,41], suggesting the existence of neutrophil–microglia crosstalk that has not to our knowledge previously been hypothesized in Alzheimer's disease. We also observed the formation of intravascular and intraparenchymal NETs, strongly suggesting that NETs may contribute to BBB damage and neuronal injury in Alzheimer's disease[42–44]. Neutrophil-dependent brain damage is also supported by our data showing that migrating neutrophils produce IL-17, which is directly toxic to neurons and the BBB and may recruit more neutrophils[32,33].

Neutrophil depletion or the blockade of integrin LFA-1 reduces pathological severity in several animal models of sterile inflammation, suggesting that neutrophil-directed therapy may also benefit Alzheimer's disease patients[30]. However, anti-integrin therapies have been previously shown to induce progressive multifocal

leukoencephalopathy in patients with autoimmune disorders, especially in immunosuppressed subjects[45]. Even so, the availability of improved tests to detect patients at risk of leukoencephalopathy[45] and the fact that Alzheimer's disease patients do not normally require immunosuppressive therapy suggests that anti-integrin strategies may still be beneficial for the treatment of Alzheimer's disease.

In conclusion, we have found a new mechanism of inflammation underlying Alzheimer's disease, highlighting the role of neutrophil trafficking in microglial activation, synaptic dysfunction, the accumulation of abnormal Aβ and tau, and memory decline. Current Alzheimer's disease therapies provide only temporary improvement and marginally reduce the rate of cognitive decline. Therefore, we propose that targeting the mechanisms of neutrophil-dependent inflammation could inhibit early pathogenesis and protect Alzheimer's disease patients from ongoing cerebral injury during the progression of the disease.

METHODS

Methods and any associated references are available in the online version of the paper.

Note: Any Supplementary Information and Source Data files are available in the online version of the paper.

ACKNOWLEDGMENTS

We thank C. Laudanna (University of Verona) for providing the reagents to measure LFA-1 integrin affinity in human neutrophils. This work was supported by funding under the European Research Council grant 261079-NEUROTRAFFICKING (G.C.), Fondazione Cariverona (G.C.) and the European Community FP7 grant 282095-TARKINAID (G.B.). S.D. received a fellowship from the Fondazione Italiana Sclerosi Multipla, Genoa, Italy.

AUTHOR CONTRIBUTIONS

G.C., E.Z and E.P. designed the experiments and analyzed the data. E.Z., E.P., V.D.B., G.P., S.B., E.T., B.R., S.A., S.D., A.M., L.M. and T.C. performed the experiments. G.B. and S.N. provided expertise in neutrophil extracellular traps. D.C. provided 129/C57BL6 mice. G.T. and L.C. analyzed the proximity between amyloid plaques and MPO^+ cells. B.B. provided human tissue samples. E.Z. and G.C. wrote the paper.

COMPETING FINANCIAL INTERESTS

The authors declare no competing financial interests.

1. Querfurth, H.W. & LaFerla, F.M. Alzheimer's disease. *N. Engl. J. Med.* **362**, 329–344 (2010).
2. Selkoe, D.J. Alzheimer's disease is a synaptic failure. *Science* **298**, 789–791 (2002).
3. Wyss-Coray, T. Inflammation in Alzheimer disease: driving force, bystander or beneficial response? *Nat. Med.* **12**, 1005–1015 (2006).
4. Schwartz, M., Kipnis, J., Rivest, S. & Prat, A. How do immune cells support and shape the brain in health, disease, and aging? *J. Neurosci.* **33**, 17587–17596 (2013).
5. Czirr, E. & Wyss-Coray, T. The immunology of neurodegeneration. *J. Clin. Invest.* **122**, 1156–1163 (2012).
6. Krstic, D. & Knuesel, I. Deciphering the mechanism underlying late-onset Alzheimer disease. *Nat. Rev. Neurol.* **9**, 25–34 (2013).
7. Kitazawa, M., Oddo, S., Yamasaki, T.R., Green, K.N. & LaFerla, F.M. Lipopolysaccharide-induced inflammation exacerbates tau pathology by a cyclin-dependent kinase 5-mediated pathway in a transgenic model of Alzheimer's disease. *J. Neurosci.* **25**, 8843–8853 (2005).
8. in t' Veld, B.A. *et al.* Nonsteroidal antiinflammatory drugs and the risk of Alzheimer's disease. *N. Engl. J. Med.* **345**, 1515–1521 (2001).
9. Szekely, C.A. & Zandi, P.P. Non-steroidal anti-inflammatory drugs and Alzheimer's disease: the epidemiological evidence. *CNS Neurol. Disord. Drug Targets* **9**, 132–139 (2010).
10. Block, M.L., Zecca, L. & Hong, J.S. Microglia-mediated neurotoxicity: uncovering the molecular mechanisms. *Nat. Rev. Neurosci.* **8**, 57–69 (2007).
11. Cagnin, A. *et al. In-vivo* measurement of activated microglia in dementia. *Lancet* **358**, 461–467 (2001).
12. Hollingworth, P. *et al.* Common variants at *ABCA7*, *MS4A6A*/*MS4A4E*, *EPHA1*, *CD33* and *CD2AP* are associated with Alzheimer's disease. *Nat. Genet.* **43**, 429–435 (2011).
13. Lambert, J.C. *et al.* Meta-analysis of 74,046 individuals identifies 11 new susceptibility loci for Alzheimer's disease. *Nat. Genet.* **45**, 1452–1458 (2013).
14. Jonsson, T. *et al.* Variant of TREM2 associated with the risk of Alzheimer's disease. *N. Engl. J. Med.* **368**, 107–116 (2013).
15. Prokop, S., Miller, K.R. & Heppner, F.L. Microglia actions in Alzheimer's disease. *Acta Neuropathol.* **126**, 461–477 (2013).
16. Zlokovic, B.V. Neurovascular pathways to neurodegeneration in Alzheimer's disease and other disorders. *Nat. Rev. Neurosci.* **12**, 723–738 (2011).
17. Rossi, B., Angiari, S., Zenaro, E., Budui, S.L. & Constantin, G. Vascular inflammation in central nervous system diseases: adhesion receptors controlling leukocyte-endothelial interactions. *J. Leukoc. Biol.* **89**, 539–556 (2011).
18. Savage, M.J. *et al.* Cathepsin G: localization in human cerebral cortex and generation of amyloidogenic fragments from the beta-amyloid precursor protein. *Neuroscience* **60**, 607–619 (1994).
19. Togo, T. *et al.* Occurrence of T cells in the brain of Alzheimer's disease and other neurological diseases. *J. Neuroimmunol.* **124**, 83–92 (2002).
20. Subramanian, S. *et al.* CCR6: a biomarker for Alzheimer's-like disease in a triple transgenic mouse model. *J. Alzheimers Dis.* **22**, 619–629 (2010).
21. Baik, S.H. *et al.* Migration of neutrophils targeting amyloid plaques in Alzheimer's disease mouse model. *Neurobiol. Aging* **35**, 1286–1292 (2014).
22. Michaud, J.P., Bellavance, M.A., Préfontaine, P. & Rivest, S. Real-time *in vivo* imaging reveals the ability of monocytes to clear vascular amyloid beta. *Cell Reports* **5**, 646–653 (2013).
23. Oakley, H. *et al.* Intraneuronal β-amyloid aggregates, neurodegeneration, and neuron loss in transgenic mice with five familial Alzheimer's disease mutations: potential factors in amyloid plaque formation. *J. Neurosci.* **26**, 10129–10140 (2006).
24. Oddo, S. *et al.* Triple-transgenic model of Alzheimer's disease with plaques and tangles: intracellular Aβ and synaptic dysfunction. *Neuron* **39**, 409–421 (2003).
25. Oddo, S., Caccamo, A., Kitazawa, M., Tseng, B.P. & LaFerla, F.M. Amyloid deposition precedes tangle formation in a triple transgenic model of Alzheimer's disease. *Neurobiol. Aging* **24**, 1063–1070 (2003).
26. Billings, L.M., Oddo, S., Green, K.N., McGaugh, J.L. & LaFerla, F.M. Intraneuronal Aβ causes the onset of early Alzheimer's disease-related cognitive deficits in transgenic mice. *Neuron* **45**, 675–688 (2005).
27. Janelsins, M.C. *et al.* Early correlation of microglial activation with enhanced tumor necrosis factor-alpha and monocyte chemoattractant protein-1 expression specifically within the entorhinal cortex of triple transgenic Alzheimer's disease mice. *J. Neuroinflammation* **2**, 23 (2005).
28. Green, K.N., Billings, L.M., Roozendaal, B., McGaugh, J.L. & LaFerla, F.M. Glucocorticoids increase amyloid-beta and tau pathology in a mouse model of Alzheimer's disease. *J. Neurosci.* **26**, 9047–9056 (2006).
29. Mastrangelo, M.A. & Bowers, W.J. Detailed immunohistochemical characterization of temporal and spatial progression of Alzheimer's disease-related pathologies in male triple-transgenic mice. *BMC Neurosci.* **9**, 81 (2008).
30. Phillipson, M. & Kubes, P. The neutrophil in vascular inflammation. *Nat. Med.* **17**, 1381–1390 (2011).
31. Kolaczkowska, E. & Kubes, P. P. Neutrophil recruitment and function in health and inflammation. *Nat. Rev. Immunol* **13**, 159–175 (2013).
32. Kebir, H. *et al.* Human TH17 lymphocytes promote blood-brain barrier disruption and central nervous system inflammation. *Nat. Med.* **13**, 1173–1175 (2007).
33. Siffrin, V. *et al. In vivo* imaging of partially reversible th17 cell-induced neuronal dysfunction in the course of encephalomyelitis. *Immunity* **33**, 424–436 (2010).
34. DiStasi, M.R. & Ley, K. Opening the flood-gates: how neutrophil-endothelial interactions regulate permeability. *Trends Immunol.* **30**, 547–556 (2009).
35. Bolton, S.J., Anthony, D.C. & Perry, V.H. Loss of the tight junction proteins occludin and zonula occludens-1 from cerebral vascular endothelium during neutrophil-induced blood-brain barrier breakdown *in vivo*. *Neuroscience* **86**, 1245–1257 (1998).
36. Kalaria, R.N. The blood-brain barrier and cerebrovascular pathology in Alzheimer's disease. *Ann. NY Acad. Sci.* **893**, 113–125 (1999).
37. Gautam, N., Herwald, H., Hedqvist, P. & Lindbom, L. Signaling via beta(2) integrins triggers neutrophil-dependent alteration in endothelial barrier function. *J. Exp. Med.* **191**, 1829–1839 (2000).
38. Ryu, J.K. & McLarnon, J.G. A leaky blood-brain barrier, fibrinogen infiltration and microglial reactivity in inflamed Alzheimer's disease brain. *J. Cell. Mol. Med.* **13**, 2911–2925 (2009).
39. Ley, K., Laudanna, C., Cybulsky, M.I. & Nourshargh, S. Getting to the site of inflammation: the leukocyte adhesion cascade updated. *Nat. Rev. Immunol.* **7**, 678–689 (2007).
40. Silva, M.T. Neutrophils and macrophages work in concert as inducers and effectors of adaptive immunity against extracellular and intracellular microbial pathogens. *J. Leukoc. Biol.* **87**, 805–813 (2010).
41. Soehnlein, O. & Lindbom, L. Phagocyte partnership during the onset and resolution of inflammation. *Nat. Rev. Immunol.* **10**, 427–439 (2010).
42. Kessenbrock, K. *et al.* Netting neutrophils in autoimmune small-vessel vasculitis. *Nat. Med.* **15**, 623–625 (2009).
43. Garcia-Romo, G.S. *et al.* Netting neutrophils are major inducers of type I IFN production in pediatric systemic lupus erythematosus. *Sci. Transl. Med.* **3**, 73ra20 (2011).
44. Allen, C. *et al.* Neutrophil cerebrovascular transmigration triggers rapid neurotoxicity through release of proteases associated with decondensed DNA. *J. Immunol.* **189**, 381–392 (2012).
45. Baldwin, K.J. & Hogg, J.P. Progressive multifocal leukoencephalopathy in patients with multiple sclerosis. *Curr. Opin. Neurol.* **26**, 318–323 (2013).

ONLINE METHODS

Reagents. The following rat anti-mouse monoclonal antibodies were purified from serum-free hybridoma media in our laboratory: anti–ICAM-1 (clone YN 1.1.7.4), anti–LFA-1 (clone TIB213 for mouse treatment and clone KIM127 for affinity studies), anti–VCAM-1 (clone MK 2.7), anti–E-selectin (clone RME-1), anti-CD45 (clone 30G12), anti-CD3 (clone145-2C11), anti-RAS (clone Y13259) and anti–Gr-1 (clone RB6-8C5). The anti–LFA-1 antibody (clone 327A) was kindly provided by K. Kikly (Eli Lilly and Co.). Anti–mouse Ly6G antibody (clone 1A8) for mouse treatment was purchased from the UCSF Monoclonal Antibody Core. The following antibodies were purchased from commercial sources: rat anti–mouse CD11a (clone M17/4, Bioxcell), APC/Cy7 anti–mouse CD11c (clone N418, BioLegend), PE-Cy7 anti–mouse Ly6C (clone AL-21, BD Pharmingen), anti–mouse IL-17 (catalog number AF-421-NA, R&D Systems), anti–mouse P-selectin (clone CD62P, BD Pharmingen), anti–mouse CD18 (clone M18/2, BioLegend), anti–mouse CD31 (clone 390, eBioscience), anti–human Aβ (clone 6E10, Covance). VioBlue anti–mouse CD45 (clone 30F11), FITC anti–human and mouse CD11b (clone M1/70.15.11.5), PE anti–mouse Gr-1 (clone RB6-8C5, used for flow cytometry studies), APC anti–mouse Ly6G (clone 1A8, used for flow cytometry studies) were from Miltenyi Biotec. The following secondary antibodies were used: biotinylated anti–rat IgG (catalog number BA-4000, Vector Labs), anti–rabbit IgG (Fc specific)-biotin antibody (catalog number SAB3700856, Sigma); anti–mouse IgG F(ab′)$_2$-biotin antibody (catalog number SAB3700995, Sigma). Avidin–Texas Red (catalog number A-2006) was from Vector labs. TNF-α and CXCL12 were purchased from R&D Systems. Polyclonal rabbit anti–human myeloperoxidase (catalog number A0398), anti–human Aβ (catalog number M0872) and fluorescence mounting medium (catalog number S3023) were purchased from Dako. MeO-X04 was kindly provided by W. Klunk, University of Pittsburgh. PTx and bocMLF were purchased from Tocris Bioscience. Cell trackers CMTPX, CMAC and the 655-nm and 525-nm non-targeted Q-dots were obtained from Molecular Probes.

Mice. We used APP/PS1 double transgenic mice with five FAD mutations (5xFAD) coexpressing the *APP* and *PS1* (*PSEN1*) transgenes at high levels using the Thy-1 promoter (Tg6799)[23]. Transgenic lines were maintained by crossing heterozygous transgenic mice with B6SJL F1 breeders. The 3xTg-AD mice expressing three mutant human transgenes—PS1 (M146V), βAPP (Swedish) and tau (P301L)[24]—were purchased from The Jackson Laboratory (Sacramento, CA). Although the 3xTg-AD mice were originally derived from a 129/C57BL6 background[24], genetic analysis showed that our 3xTg-AD mouse colony matched ~80% of the allelic profiles of C57BL/6 mice after ten generations of random mating. C57BL/6 mice were used as wild-type controls for our 3xTg-AD mice on the basis of several previous studies[46–50] and our data showing that C57BL/6 mice are suitable controls for 3xTg-AD mice in behavioral and neuropathological tests (**Supplementary Fig. 5r**,**s**). We also found that C57BL/6 and 129/C57BL6 mice from our mouse colony showed no significant differences in behavioral and neuropathological tests (**Supplementary Fig. 5r**,**s**). To investigate the role of LFA-1, 3xTg-AD mice were crossed with LFA-1-deficient mice (*Itgal*$^{-/-}$), which are on the C57Bl/6 genetic background. After nine generations, the resulting LFA-1-deficient Alzheimer's disease model mice had a near-isogenic C57BL/6 genetic background. Animals were housed in pathogen-free, climate-controlled facilities and were provided with food and water *ad libitum*. All mice were housed and used in according to current European Community laws. All mouse experiments were carried out in accordance with guidelines prescribed by the Ethics Committee for the usage of laboratory animals for research purposes at the University of Verona and by the Italian Ministry of Health.

Neutrophil preparation. Mouse neutrophils were isolated by the centrifugation of bone marrow cells flushed from femurs and tibias over a Percoll discontinuous density gradient. More than 90% of the isolated cells were Ly6G$^+$ neutrophils as determined by flow cytometry (data not shown). Following isolation, neutrophils were resuspended at a density of 10×10^6 per ml in HBSS supplemented with 0.5 mM $CaCl_2$ and 5 mM D-glucose (HGCa). Human neutrophils were prepared from the buffy coats of healthy volunteers by centrifugation through Ficoll Paque Plus. Donors provided their informed consent before samples were taken. Contaminating erythrocytes were removed by Dextran500 sedimentation followed by hypotonic lysis. After isolation, cells were suspended in HGCa at a density of 10×10^6 per ml.

Immunofluorescence staining. Sections were taken from the anterior hippocampus through the bregma – 2.9 mm at an intersection interval of 500 µm (every fourth section). Frozen mouse brains fixed in 4% paraformaldehyde (PFA) were cut into 30-µm coronal sections. Free-floating sections were incubated in blocking buffer for 1 h at room temperature and then with primary antibody for 18 h at 4 °C at the following concentrations: 40 µg/ml anti–VCAM-1, 10 µg/ml anti–ICAM-1, 10 µg/ml anti–P-selectin, 5 µg/ml anti–E-selectin, 5 µg/ml anti-CD45, 1 µg/ml anti-CD11c, 5 µg/ml anti-CD3, 5 µg/ml anti–Gr-1. Sections were rinsed with PBS, stained for 3 min at room temperature with 0.1% thioflavin S solution in PBS and then incubated with 7.5 µg/ml biotinylated secondary antibody at room temperature for 1 h. After rinsing in PBS, the slices were treated with 25 µg/ml avidin–Texas Red in PBS at room temperature in the dark for 1 h. Finally, the sections were incubated with 1 µg/ml DAPI for 8 min in the dark, transferred to glass slides and mounted with Dako medium. Images were acquired on a tandem confocal scanning SP5 microscope (Leica, Germany).

Quantitative analysis of fluorescent cells by confocal microscopy. Images were acquired from mouse brain sections using an SP5 tandem confocal scanning microscope (Leica, Germany) equipped with a 40× objective lens and a pinhole setting corresponding to a focal plane thickness of less than 1 µm. Eight 30-µm sections were taken every fourth section from each mouse brain starting from the anterior hippocampus. Eight random acquisition areas were considered for each brain section. To exclude false positives caused by the overlay of signals from different cells, each area was analyzed by moving through the entire *z* axis. Fluorescent Gr-1$^+$ cells were counted in a blinded fashion using Imaris software. Nonspecific staining was avoided by excluding structures less than 6 µm in diameter (1 µm = 0.3765 pixels).

Immunofluorescence staining of NETs. We used non-perfused mouse brains fixed in 4% PFA and cut into 30 coronal sections. Human and mouse brain sections were incubated in blocking buffer for 2 h at room temperature and then treated with the following primary antibodies: 5 µg/ml anti–neutrophil elastase (NE, catalog number ab68672, Abcam) for 2 h at 37 °C, 5 µg/ml anti-myeloperoxidase (MPO, catalog number AF3667, R&D) and 1 µg/ml anti-histone H3 citrulline 2+8+17 (H3-cit, catalog number ab5103, Abcam) overnight at 4 °C. We performed double staining with MPO plus NE and with MPO plus H3cit on mouse and human brain sections. After washing with 0.05% Tween-20 in PBS, we added a fluorophore-conjugated secondary antibody (anti–Alexa 488, anti–Alexa 680; Molecular Probes, Invitrogen) in blocking solution. Nuclei were stained with 1 µg/ml DAPI (Sigma) for 8 min in the dark. Finally, the sections were washed with PBS, transferred to glass slides and mounted with Dako medium. Glass slices were kept at 4 °C in the dark and analyzed using an SP5 confocal scanning microscope (Leica, Germany).

Aβ preparation. $Aβ_{1–42}$ was purchased from Bachem AG. Oligomeric Aβ was prepared as reported previously[51]. Briefly, after the removal of hexafluoroisopropanol, $Aβ_{1–42}$ was dissolved in DMSO to a concentration of 5 mM and diluted in F12 medium to 100 µM. After incubation for 24 h at 4 °C, the Aβ solution was centrifuged at 15,000*g* for 10 min at 4 °C and the supernatant, containing soluble oligomeric Aβ, was collected and quantitated using a MicroBCA assay (Pierce). For the preparation of fibrillar Aβ, 5 mM $Aβ_{1–42}$ in DMSO was diluted to 200 µM in 100 mM HEPES buffer (pH 7.5) and incubated for 1 week at 37 °C. After aging, the Aβ sample was centrifuged at 15,000*g* for 10 min at room temperature and the supernatant was removed. The pellet fraction was redissolved in HEPES buffer and quantitated using the MicroBCA assay. The identity of fibrillar and oligomeric Aβ was confirmed by electrophoresis as previously described[51].

Isolation of brain leukocytes and flow cytometry analysis. Mice were anesthetized and perfused through the left cardiac ventricle by injection of cold PBS. The brain was digested with 20 U/ml of DNase I and 1 mg/ml collagenase at 37 °C for 45 min. Cells were isolated by passing the digested tissue through a 70-µm cell strainer, resuspended in 30% Percoll and loaded onto 70% Percoll. Tubes were then centrifuged at 1,300*g* for 20 min at 4 °C. Cells

doi:10.1038/nm.3913

were removed from the interphase, washed and labeled with the following anti-mouse antibodies: anti-CD45–Vioblue (catalog number 130-092-910); anti-CD11b–FITC (catalog number 130-081-201); anti–Gr-1–PE (catalog number 130-091-932); anti-Ly6G–APC (catalog number 130-093-140) (Miltenyi Biotec). Cells were acquired by flow cytometry with MACSQuant Analyzer (Miltenyi Biotec). Data were analyzed using FlowJo software. The procedure is shown in **Supplementary Figure 3**.

Isolation of blood leukocytes and flow cytometry. Blood was collected from the retro-orbital plexus and mixed with PBS containing 10 U/ml heparin and 4% dextran. After incubation at room temperature for 1 h, the supernatant was centrifuged and cells were labeled at room temperature for 45 min with the following anti-mouse antibodies: anti-CD45–Vioblue, anti-CD11b–FITC, anti-Ly6C–PE/Cy7 (catalog number 560593, BD Pharmingen) and anti-Ly6G–APC. Red cells were lysed in lysis buffer for 10 min and the remaining leukocytes were washed and acquired by flow cytometry using a MACSQuant Analyzer (Miltenyi Biotec). Data were analyzed using FlowJo software.

Surgical preparations for TPLSM. Mice were anesthetized and the core body temperature was monitored and maintained using a regulated heating pad. Hair on the scalp was removed with an electric razor. The scalp was then sterilized with alcohol. An incision was made along the midline of the scalp to expose the skull overlying the cortical region of interest. A 1-mm-diameter region of skull was thinned using a high-speed micro drill and a stainless steel burr. Drilling was halted every few seconds to prevent heating and bone dust was removed using a compressed air canister. Care was taken not to deflect the skull during drilling. Animals showing any signs of damage, such as subdural or epidermal bleeding, were excluded from use. Mice were given a bolus of warm saline for rehydration and were allowed to recover from anesthesia on a water-circulating heating pad. Neutrophils were isolated from bone marrow and labeled with the fluorescent cell trackers CMTPX or CMAC. Videos were acquired at 18–24 h after intravenous injection of the cells. To visualize blood vessels, 525-nm non-targeted Q-dots were injected intravenously. Mice were kept under anesthesia using 1.5% isoflurane with a facemask.

TPLSM acquisition and data analysis. Time-lapse imaging was performed using a SP5 tandem confocal scanning microscope (Leica, Germany). Each plane represents an image 525 × 525 µm (*xy* dimensions), and approximately 22–44 sequential planes were acquired at 2.5-µm increments in the *z* dimension to obtain *z*-stacks. The *z*-stacks were acquired every 32–63 s during time-lapse recordings. Image reconstruction, multidimensional rendering and manual cell tracking were carried out using Imaris software (Bitplane). Neutrophil movement analysis was carried out using functions of the T cell analysis (TCA) software (J. Dempster, University of Strathclyde, Glasgow, Scotland). One hundred cells per group were manually tracked over time from maximum-intensity, top-view image sequences. Tracks >6 min (β12 time points) were included in the analysis. Instantaneous velocities were calculated from the distance moved between successive time points (<30 s each). Cell velocities were reported as the mean of instantaneous velocities in each cell track. Motility coefficients (μm^2/min) were calculated for individual tracks by linear regression of displacement^2 versus time point with T cell analysis software. The meandering index for a cell track was computed as the displacement between the initial and final points on each the track divided by the total length of the random path. Data were transferred and plotted in GraphPad Prism v5.0 (Sun Microsystems).

Rapid adhesion assays. Eighteen-well glass slides were coated for 16 h at 4 °C with human fibrinogen (20 µg/well in endotoxin-free PBS) or with purified human ICAM-1 (3,000 sites/μm^2)[52]. Neutrophils (10^5 per well; 5×10^6 per mL in 10% FCS, 1 mM $CaCl_2$/$MgCl_2$ in PBS, pH 7.2) were added, incubated for 10 min at 37 °C, and then stimulated by the addition of agonist for 2 min before washing, fixing on ice in 1.5% glutaraldehyde for 60 min, and computer-assisted enumeration[52] of cells bound in 0.2 mm^2. When required, cells were preincubated for 20 min with 100 µM boc-MLF or for 2 h with 2 µg/ml PTx at 37 °C.

Measurement of LFA-1 affinity states. Human neutrophils resuspended in standard adhesion buffer at 2×10^6 per mL were briefly preincubated with 10 µg/ml of monoclonal antibody KIM127 to study the extended conformation epitope corresponding to an intermediate-affinity state of LFA-1 or 327A to study the high-affinity state[52]. The cells were stimulated for 10 s with 0.5 µM CXCL12, 0.1 µM fMLP, or 20 µM $A\beta_{1-42}$ or $A\beta_{42-1}$ while stirring at 37 °C. After rapid washing, cells were stained with FITC-conjugated secondary polyclonal antibody and analyzed by cytofluorimetric quantification.

Quantification of reactive oxygen species. Isoluminol-based chemiluminescence assays were prepared in Hank's balanced salt solution supplemented with 0.5 mM $CaCl_2$ and 5 mM D-glucose (HGCa) in the presence of horseradish peroxidase (HRP) and isoluminol in a temperature-controlled Multilabel Count Victor X5 (PerkinElmer). The assays were carried out in dark 96-well plates precoated with 250 µg/ml human fibrinogen in HGCa containing 100 µM isoluminol and 8 U/ml HRP[53,54]. Following the addition of 1×10^5 human neutrophils or 7.5×10^5 mouse neutrophils, the plates were left at 37 °C for 10 min and the reaction initiated by introducing the stimulus (see text for concentrations). Light emission was recorded once per minute.

Detection of adhesion molecules by immunofluorescence staining of bEnd.3 cells stimulated with $A\beta_{1-42}$ soluble oligomers. The bEend.3 cell line is an endothelial line derived from the mouse cerebral cortex obtained from the ATCC (CRL-2299). The cells were authenticated by expression of von Willebrand factor (ATCC) and CD31 expression (**Supplementary Fig. 1k**) and were tested for mycoplasma contamination with the MycoTracer PCR detection kit (catalog number FA30Q05120, PAA—The Cell Culture Company, Austria). The cells were seeded at a density of 2×10^4 per ml on glass coverslips in 24-well plates containing Dulbecco's modified Eagle's medium (DMEM) supplemented with 10% FCS. The cells were stimulated with 10 µM soluble oligomeric $A\beta_{1-42}$, for 18 h in DMEM plus 1% FCS. As a positive control, the cells were treated with 25 U/ml TNFβ for 18 h in DMEM plus 1% FCS. The cells were then rinsed with phosphate-buffered saline (PBS) and fixed in 4% PFA in PBS for 10 min. After washing in PBS, the cells were incubated with blocking solution at room temperature for 1 h, and then overnight at 4 °C with the primary antibody at the following concentrations: anti-VCAM-1, 50 µg/ml; anti-ICAM-1, 10 µg/ml; anti-CD31, 0.5 µg/ml; anti-E-selectin, 5 µg/ml; and anti-P-selectin, 1.5 µg/ml. The cells were then rinsed with PBS, incubated with 7.5 µg/ml biotinylated secondary antibody at room temperature for 1 h and with 25 µg/ml avidin–Texas Red at room temperature for 1 h. Finally, the cells were stained with 1 µg/ml DAPI for 5 min in the dark. The slides were mounted with Dako and analyzed by fluorescence microscopy (DM6000B Leica Microsystems GmbH). Images were acquired by using a Leica DC500 digital camera and the Leica Application Suite software. The viability of bEnd.3 cells was determined by measuring their metabolic activity using WST-1 (Roche) according to the manufacturer's instructions.

Quantitative analysis of fluorescent endothelial adhesion molecules. The expression of adhesion molecules and CD31 was analyzed by fluorescent surface and intensity computing using Imaris software (Bitplane). Images of bEnd.3 cells were acquired using a fluorescence microscope with a constant exposure time determined by staining with secondary antibodies alone. All images were acquired within the linear intensity range 0–4,095 (ref. 55). The fluorescence of the adhesion molecules and CD31 was measured using the same threshold and the averages were determined (3–5 images per condition from two independent experiments)[56]. Differences in the nuclear size distribution (area) between untreated (control) and Aβ-treated bEend.3 cells were determined by analyzing five images of 300–400 cells for each condition, and measuring the DAPI fluorescence of each nucleus.

Images were acquired from mouse brain sections using a confocal microscope equipped with a 20× objective lens at a constant exposure time. The analysis was blinded and carried out using four nonconsecutive sections for each condition as described for microglia quantification. Background intensity based on images stained with secondary antibodies alone was subtracted. To exclude nonspecific staining, structures less than 5.5 µm in diameter (1 µm = 0.18825 pixels) were excluded. The total positive vessel volume and intensity was averaged from six (hippocampal region) to 15 (meningeal region) images per slice and compared to age-matched control mice and the 3xTg-AD or 5xFAD groups[55].

Treatment of mice. Anti-Ly6G antibody (1A8 clone, specific for neutrophils) and anti–Gr-1 antibody (RB6-8C5 clone, which recognizes neutrophils but also other leukocyte subpopulations) were used to induce depletion of neutrophils from the peripheral circulation. Anti–LFA-1 (TIB213 or M17/4) antibodies were used to block integrin LFA-1. Anti-Ras (Y13259) antibody was used as a control. Antibodies were diluted to 1 mg/mL in sterile endotoxin-free PBS. Mice were injected i.p. with 0.5 mg of each antibody for the first treatment. They were then injected with 300 µg of antibodies i.p. every second day. Treatment was continued for 4 weeks until behavioral testing. Blood neutrophils levels remained low (0–1% of blood leukocytes in treated mice, versus 8–12% in controls) when measured. Mice were sacrificed after behavioral assessment. Hemi-brains were cut into sagittal sections without the hindbrain and flash-frozen on dry ice for subsequent protein extraction. The matching hemi-brains were fixed in 4% PFA for 24 h then cut into sections using a cryostat.

Y-maze test. Spontaneous alternation rates were assessed using a symmetrical Y-maze built from black plastic material with three arms arranged at 120° extending from a central space. During 8-min test sessions, each mouse was placed in one arm and allowed to explore freely through the maze. The sequence and total number of arms entered was recorded. Alternation was defined as successive entries into the three arms in overlapping triple sets. The alternation percentage was calculated as the number of triads containing entries into all three arms/maximum possible alternations (the total number of arms entered − 1) × 100. To diminish odor cues, the maze was cleaned with 70% ethanol solution. Experiments were blinded with respect to the genotype of the mice.

Contextual fear conditioning test. Contextual fear conditioning was performed in 30 × 24 × 21 cm operant chambers (Ugo Basile). Each chamber was equipped with a floor of stainless steel rods through which a footshock could be administered, two stimulus lights, one house light and a solenoid, all controlled by ANY-maze computer software (Stoelting). Mice were trained and tested on 2 consecutive days. Training consisted of placing a subject in a chamber, illuminating stimulus and house lights, and allowing exploration for 2 min. A 15-s tone stimulus (2 Hz) then ended together with 2-s foot shock (1.5 mA). The pairing of stimuli was repeated twice at 2-min intervals. Thirty seconds after the second shock, the mice were removed from the chamber. After a further 20 h, mice were placed back into the same training chamber for context, and the contextual conditioning test without tone or shock was carried out for 5 min, with freezing behavior recorded by the experimenter. Freezing was defined as lack of movement except that required for respiration. At the end of the 5 min contextual test, mice were returned to their home cage. Approximately 2 h later, mice were placed in a novel environment for 3 min without any stimulus presentation. The auditory cue was then presented for 3 min, and freezing was again scored. The freezing score was expressed as a percentage for each portion of the test. Memory for the context for each subject was obtained by subtracting the percentage of freezing in the novel environment from that in the context. Experiments were blinded with respect to the genotype of the mice.

Histopathological analysis. Mouse hemi-brains were cut into 30-µm coronal sections. Free-floating sections were fixed for 10 min in 4% PFA. For microglia staining, we used anti–mouse ionized calcium binding adaptor molecule-1 antibody (Iba-1, catalog number 019-19741, Wako). Brain sections were treated with 2% normal goat serum (Vector) and 0.4% Triton and then incubated for 18 h at 4 °C with 1 µg/ml of the following primary antibodies: anti–Iba-1 for microglial staining and mouse anti-Aβ (6E10, Covance). For Aβ staining, the sections were treated with 70% formic acid for 20 min for epitope retrieval. After washing with 0.05% Tween-20 in PBS, we added 3% H_2O_2 for 10 min at room temperature before washing the sections and incubating them in 4 µg/ml of the biotinylated secondary antibody (goat anti-rabbit and goat anti-mouse, Sigma). The immunoreactivity was visualized using the Vectastain ABC kit (Vector) for 30 min and Vector NovaRED (Vector) as the chromogen for 3 min at room temperature. Finally, brain portions were washed with distilled water, transferred to glass slides, dehydrated in 95% and 100% ethanol for 1 min each and mounted with Eukitt mounting medium (Sigma). Images were acquired using a fluorescence microscope (DM6000B, Leica).

Quantification of microglia and amyloid load. The numerical density of Iba-1$^+$ immunoreactive microglia and the area of amyloid plaques, stained with Aβ clone 6E10 antibody, were determined in coronal sections throughout the cortex and the dorsal hippocampus of both 3xTg-AD and wild-type control mice. Sections were taken from the anterior hippocampus through the bregma − 2.9 mm at an intersection interval of 500 µm (every fourth section) to analyze the whole area of the cortex and the hippocampus. The specific areas were the parietal cortex, the dentate gyrus and the CA1 area of the hippocampus. Iba-1$^+$ microglia were visualized using a LEICA fluorescence microscope (DM6000B, Leica) and counted blindly with ImageJ v1.32j software.

Quantitative analysis of mouse fluorescent cells by confocal microscopy. Images were acquired from mouse brain sections using a scanning confocal microscope (SP5, Leica, Germany) equipped with a 40× objective lens and a pinhole setting corresponding to a focal plane thickness of less than 1 µm. Eight sections of 30 µm thickness were taken every fourth section for each mouse brain starting from the anterior hippocampus. Eight random acquisition areas were considered for each brain section. To exclude false positives caused by to the overlay of signals from different cells, each area was analyzed by moving through the entire *z* axis[57]. Fluorescent CD45$^+$ or Ly6G$^+$ cells were counted in a blinded fashion using Imaris software. Nonspecific staining was avoided by excluding structures less than 6 µm in diameter (1 µm = 0.3765 pixels).

Hematoxylin and eosin staining and naphthol AS-D chloroacetate esterase staining. All material was collected from donors for or from whom a written informed consent for a brain autopsy and the use of the material and clinical information for research purposes had been obtained by the MRC London Brain Bank for Neurodegenerative Diseases, which belongs to BrainNet Europe (http://www.brainnet-europe.org/). Brain samples were fixed in 4% PFA and embedded in paraffin (human brain samples). Polymorphonuclear cells were identified by staining human and mouse brain sections for chloroacetate esterase, a neutrophil-specific marker (naphthol AS-D chloroacetate esterase kit, Sigma-Aldrich). We also stained brain sections with hematoxylin and eosin using standard protocols.

Aβ extraction. Frozen mouse hemi-brains were weighed and homogenized in 1 ml TBS (120 mM NaCl, 50 mM Tris, pH 8.0) containing complete protease inhibitor (Roche Applied Science) and phosphatase inhibitor cocktail 2 (Sigma) using a Dounce homogenizer. The homogenates were then sonicated and centrifuged at 80,000*g* for 1 h at 4 °C. The supernatant (TBS-soluble fraction) was removed and stored at −80 °C. The pellet was redissolved in 0.5 ml TBS containing 2% SDS, sonicated, and centrifuged at 80,000*g* for 1 h at 4 °C. The supernatant (SDS-soluble fraction) was frozen at −80 °C. The resulting pellets were resuspended in 0.5 ml 70% formic acid, sonicated, and centrifuged at 80,000*g* for 1 h at 4 °C, and the supernatant was neutralized using 1 M Tris at pH 11. Protein concentrations were determined using the Bradford protein assay. In some experiments, four-step extraction of Aβ was performed. Frozen hemi-brains were sequentially extracted in four steps as previously described[58].

Sandwich ELISA for $A\beta_{1-42}$ detection. Brain extracts from transgenic or non-transgenic mice were analyzed by sandwich ELISA using an antibody to $A\beta_{37-42}$ (catalog number ab34376, Abcam) for capture and 6E10 antibody for detection to measure $A\beta_{1-42}$ production. The TBS extracts were diluted 1:10 and the 2% SDS extracts were diluted at least 1:20 so that Aβ was captured in EC buffer (PBS containing 1% BSA, 0.05% Tween-20). Formic acid extracts were neutralized initially by dilution 1:20 in 1 M Tris phosphate buffer, pH 11. Samples were acquired with a Victor3 1420 multilabel counter (PerkinElmer) and analyzed using Wallac 1420 software. The Aβ concentration was calculated by comparing the sample absorbance with the absorbance of known concentrations of synthetic $A\beta_{1-42}$ standard assayed in the same plate. Using the wet weight of brain in the original homogenate, the final values of Aβ in brain were expressed as nanograms per gram of wet weight brain tissue.

Immunoblotting. Frozen hemi-brains were homogenized in T-per (Thermo Fisher Scientific, Rockford, IL) extraction buffer (150 mg/ml), containing protease inhibitor (Complete Mini Protease Inhibitor Tablets, Roche Diagnostics

doi:10.1038/nm.3913

GmbH, German) and phosphatase inhibitor cocktail 2 (Sigma-Aldrich, St. Louis, MO). Homogenates were centrifuged at 80,000*g* for 1 h at 4 °C. Supernatants were collected as the detergent-soluble fraction and stored at −80 °C. The protein concentration was determined using the Bradford assay and 50 µg of protein was loaded per lane for electrophoresis on a 10% denaturing Tris/glycine SDS polyacrylamide gel before transfer to a Hybond ECL nitrocellulose membrane (Amersham Pharmacia Biotech). Membranes were blocked in 5% nonfat dry milk in TBS (pH 7.5) supplemented with 0.1% Tween-20 (TBS-T) for 1 h, followed by overnight incubation with the primary antibody in 5% BSA TBS-T. Membranes were then washed in TBS-T and incubated for 1 h with horseradish peroxidase (HRP)-conjugated anti–mouse or anti–rabbit IgG (Amersham Pharmacia Biotech) in 3% BSA in TBS-T. Bound HRP-conjugated secondary antibody was detected with the ECL system (Millipore). The following primary antibodies were used: HT7 (total human tau, 1:1,000; Thermo Scientific, clone MN1000), AT8 (phosphorylated tau at Ser202/Thr205, 1:500; Thermo Scientific, clone MN1020), anti–β-actin polyclonal antibody (rabbit, 1:5,000, catalog number A2066, Sigma), anti–β-actin monoclonal antibody (mouse, 1:10,000; catalog number A1978, Sigma), anti-synaptotagmin (catalog number 3337, Cell Signaling) and anti-PSD95 (rabbit, 1:1,000; catalog number 3450, Cell Signaling). The optical intensity of bands representing phosphorylated tau, tau and synaptic proteins was determined with a GS-710 densitometer (Bio-Rad) using Quantity One software (Bio-Rad) and normalized against α-actin.

Immunofluorescence staining of human brain tissue. Paraffinated brain autopsy samples from 11 sporadic human Alzheimer's disease patients and 11 aged-matched controls were obtained from the MRC London Brain Bank for Neurodegenerative Disease and used for immunofluorescence staining. Information on human subjects is provided in **Supplementary Table 1**. Paraffinated brain tissues were processed for immunofluorescence staining. Hippocampal and cortical sections were labeled with polyclonal rabbit anti–human myeloperoxidase (catalog number A 0398, Dako) and anti–human Aβ (catalog number M 0872, Dako). NETs staining was performed as described above. After washing, appropriate biotinylated secondary antibody (Vector) and fluorophore-conjugated secondary antibody were added. Nuclei were stained with DAPI.

Quantification of MPO$^+$ cells. Images were acquired from human brain slices using an SP5 tandem confocal scanning microscope at a magnification of 10× with a resolution of 1,024 × 1,024 pixels (1,240 × 1,240 µm area). Cells were counted in a blinded fashion in three sections for each brain. Ten images were acquired randomly in a blinded fashion for each section with a median *z*-volume of 40 µm. The results were expressed as a mean value of the absolute number of cells per acquisition field or the total number of cells for each brain (**Supplementary Table 1**). The cells were counted in six phases using ImageJ software: background subtraction, color deconvolution, brightness threshold for acquiring a binary image, Gaussian blur for smoothening the threshold, watershed segmentation of cells touching each other and analysis of the particles to determine the cell count.

Analysis of the proximity between MPO$^+$ cells and amyloid plaques. Images were acquired from human brain slices using an SP5 tandem confocal scanning microscope at a magnification of 40×. Only MPO$^+$ cells with a nucleus visualized by DAPI staining were considered. Plaques were stained with the 6F/3D antibody and a plaque volume range of 200–900 µm^3 was selected for analysis. Image reconstruction, cell surface analysis and measurements were carried out using Imaris software (Bitplane). The distance between each MPO$^+$ cell and the adjacent plaque was measured for a total of 105 cells. We recorded the *x*, *y* and *z* coordinates of the MPO$^+$ cells and plaques from 44 random *z*-stacks of images (four for each brain) by using the surface function of Imaris. The data were imported into the statistical analysis software R. The modeled data were generated by randomly assigning coordinates to each MPO$^+$ cell and plaque measured in a 388 × 388 × 15 µm volume while assuming a random spatial relationship between MPO$^+$ cells and plaques (Monte Carlo simulation).

Statistics. A two-tailed Student's *t*-test was used for the statistical comparison of two samples. Multiple comparisons were carried out with Kruskal-Wallis test with the Bonferroni correction of *P*. For two-photon analysis, non-normally distributed data were presented as mean and compared using the Mann-Whitney *U*-test (two groups) or ANOVA followed by a suitable multiple comparison procedure (Dunn's or Dunnett's test). The Anderson-Darling test and Pearson's chi-squared test were used to compare the distribution of the distances between MPO$^+$ cells and plaques to random distances generated using Monte Carlo simulations.

46. Sterniczuk, R., Antle, M.C., Laferla, F.M. & Dyck, R.H. Characterization of the 3xTg-AD mouse model of Alzheimer's disease: part 2. Behavioral and cognitive changes. *Brain Res.* **1348**, 149–155 (2010).
47. Halagappa, V.K. *et al.* Intermittent fasting and caloric restriction ameliorate age-related behavioral deficits in the triple-transgenic mouse model of Alzheimer's disease. *Neurobiol. Dis.* **26**, 212–220 (2007).
48. Nakashima, A.S., Oddo, S., Laferla, F.M. & Dyck, R.H. Experience-dependent regulation of vesicular zinc in male and female 3xTg-AD mice. *Neurobiol. Aging* **31**, 605–613 (2010).
49. Robertson, R.T. *et al.* Amyloid-beta expression in retrosplenial cortex of triple transgenic mice: relationship to cholinergic axonal afferents from medial septum. *Neuroscience* **164**, 1334–1346 (2009).
50. España, J. *et al.* Intraneuronal β-Amyloid accumulation in the amygdala enhances fear and anxiety in Alzheimer's disease transgenic mice. *Biol. Psychiatry* **67**, 513–521 (2010).
51. Kim, H.J. *et al.* Selective neuronal degeneration induced by soluble oligomeric amyloid beta-protein. *FASEB J.* **17**, 118–120 (2003).
52. Bolomini-Vittori, M. *et al.* Regulation of conformer-specific activation of the integrin LFA-1 by a chemokine-triggered Rho signaling module. *Nat. Immunol.* **10**, 185–194 (2009).
53. Lundqvist, H. & Dahlgren, C. Isoluminol-enhanced chemiluminescence: a sensitive method to study the release of superoxide anion from human neutrophils. *Free Radic. Biol. Med. (Paris)* **20**, 785–792 (1996).
54. Fumagalli, L. *et al.* Class I phosphoinositide-3-kinases and SRC kinases play a nonredundant role in regulation of adhesion-independent and -dependent neutrophil reactive oxygen species generation. *J. Immunol.* **190**, 3648–3660 (2013).
55. Flister, M.J. *et al.* Inflammation induces lymphangiogenesis through up-regulation of VEGFR-3 mediated by NF-κB and Prox1. *Blood* **115**, 418–429 (2010).
56. Kook, S.-Y. *et al.* $A\beta_{1-42}$-RAGE interaction disrupts tight junctions of the blood–brain barrier via Ca^{2+}-calcineurin signaling. *J. Neurosci.* **32**, 8845–8854 (2012).
57. Ohira, K., Takeuchi, R., Iwanaga, T. & Miyakawa, T. Chronic fluoxetine treatment reduces parvalbumin expression and perineuronal nets in gamma-aminobutyric acidergic interneurons of the frontal cortex in adult mice. *Mol. Brain* **6**, 43 (2013).
58. Kawarabayashi, T. *et al.* Age-dependent changes in brain, CSF, and plasma amyloid β protein in the Tg2576 transgenic mouse model of Alzheimer's disease. *J. Neurosci.* **21**, 372–381 (2001).